PCCP

Accepted Manuscript

ROYAL SOCIETY OF CHEMISTRY

www.rsc.org/pccp

Effect of the LHCII Pigment-Protein Complex Aggregation on Photovoltaic Properties of Sensitized TiO_2 Solar Cells

Yiqun Yang [1], Ryszard Jankowiak [1,], Chen Lin [1], Krzysztof Pawlak[2], Michael Reus[2], Alfred R. Holzwarth [2], and Jun Li [1,*]*

[1] Department of Chemistry, Kansas State University, Manhattan, KS 66506;

[2] Max-Planck-Institute for Chemical Energy Conversion (MPI-CEC), D-45470 Mülheim a.d. Ruhr, Germany

ABSTRACT

A modified dye-sensitized solar cell consisting of a thin TiO_2 barrier layer sensitized with natural trimeric light-harvesting complex II (LHCII) from spinach was used as a biomimetic model to study the effects of LHCII aggregation on the photovoltaic properties. The aggregation of individual trimers induced molecular reorganization, which dramatically increased the photocurrent. The morphology of small- and large-size LHCII aggregates deposited on a surface was confirmed by atomic force microscopy. Enhanced LHCII immobilization was accomplished via electrostatic interaction with amine-functionalized photoanodes. The photocurrent responses of the assembled solar cells under illumination at three characteristic wavelength bands in the UV-Vis absorption spectra of LHCII solutions confirmed that a significant photocurrent was generated by LHCII photosensitizers. The enhanced photocurrent by large aggregated LHCII is shown to correlate with the quenching in the far-red fluorescence deriving from chlorophyll-chlorophyll charge transfer states that are effectively coupled with the TiO_2 surface and thus inject electrons into the TiO_2 conduction band. The large aggregated LHCII with more chlorophyll-chlorophyll charge transfer states is a much better sensitizer since it injects electrons more efficiently into the conduction band of TiO_2 than the small aggregated LHCII mostly consisting of unquenched chlorophyll excited state. The assembled solar cells demonstrated remarkable stability in both aqueous buffer and acetonitrile electrolytes over 30 days.

KEYWORDS Light harvesting complex II, charge transfer state, sensitized solar cell, photosynthesis, chlorophyll pigments

INTRODUCTION

Photosynthesis involves delicate systems that are designed by nature to convert solar energy into chemical energy. These systems are large supercomplexes consisting of smaller pigment-protein complexes, including membrane-associated light-harvesting antenna complexes (LHCs) for photon capture and energy transfer, as well as reaction center (RC) complexes for charge separation (CS) and photosynthetic reactions. The fundamental understanding of the light harvesting and energy-conversion processes in photosystems provides great inspiration for building low-cost high-efficiency artificial devices.[1-3] It is known that the photon energy absorbed by LHCs is transferred by ultrafast energy transfer processes to the RCs where a series of electron transfer (ET) steps take place. The redox equivalents created, together with ATP, are then converted in a series of dark reactions into chemical energy.

Light harvesting complex II (LHCII) is the most abundant chlorophyll-protein complex in nature and the major antenna complex in photosystem II (PSII). The largest PSII supercomplex, $C_2S_2M_2$, consists of a dimeric core complex (C_2) containing RCs, 4 monomeric minor antenna complexes, 4 strongly attached LHCII trimers (S_2 and M_2), and 3 to 4 loosely attached LHCII trimers.[4] Figure 1A shows the top and side views of the crystal structure[5] of an isolated LHCII trimer and its physical dimensions. The LHCII trimer consists of three monomers each of which comprises a polypeptide of about 232 amino-acid residues, 8 Chl *a* and 6 Chl *b* molecules, 3-4 carotenoids and one phospholipid.[5] LHCII not only has a primary role in light harvesting and transferring the excitation energy to the RC, but is also critical in photosynthesis regulation through photoprotective mechanisms called non-photochemical quenching (NPQ).[4, 6-11] LHCII protein aggregation was proposed to be one of the mechanistic factors controlling the dissipation

of excess photo-excited state energy of chlorophylls during NPQ (see e.g. reference[12] as a review and references therein).

Dye sensitized solar cells (DSSCs) as a mimic of natural photosynthesis, first proposed by O'Regan and Grätzel [13], have emerged as a credible alternative to conventional solar cells. A wide bandgap semiconductor layer (typically a mesoporous film made of sintered TiO_2 nanoparticles) sensitized with a visible light absorbing organic dye forms the core of the DSSC. In contrast to conventional photovoltaic devices, the CS takes place by injecting electrons from the excited dye molecules into the semiconductor layer followed by electron diffusion in the TiO_2 network. Over the past two decades, extensive research on DSSCs has been carried out by exploring various individual components and novel device architectures.[14-18] A power conversion efficiency of up to ~12% was achieved with a porphyrin-sensitized solar cell using a cobalt (II/III)-based redox electrolyte.[19] A novel organic-inorganic hybrid perovskite dye $CH_3NH_3PbI_3$ was reported to promote the DSSC efficiency to ~15% by means of sequential deposition.[20] As effective photon-to-electron conversion systems, DSSCs could be model devices to supplement spectroscopic techniques for the study of fundamental photon capture and ET properties of different photosynthetic pigment-protein complexes.

Studies have been carried out to utilize the ET processes by a direct anchoring of RCs[21, 22], LHI-RC core complexes[23], or whole photosystems (PSI or PSII)[21, 24] on gold electrodes. In a different approach, natural pigments or extracted LHCs have been used as photosensitizers to interface with a ~10 μm-thick mesoporous TiO_2 film or ZnO nanowires in fabricating DSSCs.[25-28] In such systems, the CS occurs at the sensitizer/TiO_2 interface to generate photocurrents in analogue to the function of RCs. Photocurrent enhancement was observed in LHCII incorporated DSSCs, which demonstrated the feasibility of LHCII as a photosensitizer.[26, 27] However, little is

known about the effects of LHCII aggregation on the photovoltaic and sensitization characteristics. In contrast to isolated LHCII trimers, the Chl excited states in the aggregates are strongly quenched by the formation of chlorophyll-chlorophyll charge transfer (CT) states whose presence in aggregated LHCII was independently studied recently via high-resolution hole-burning (HB) spectroscopy.[29] If the Chl-Chl CT states in the LHCII can be coupled with the TiO_2 surface, it would enhance electron injection into the TiO_2 conduction band. In this study, we compare the effects of different sizes of LHCII aggregates to illustrate the contribution of aggregation induced CT states to the photovoltaic performance using a model nanoscale thin-film TiO_2 DSSC (schematically shown in Figure 1B), and aim to reveal if there is any correlation between the surface coverage/sizes of aggregates and the photovoltaic performance.

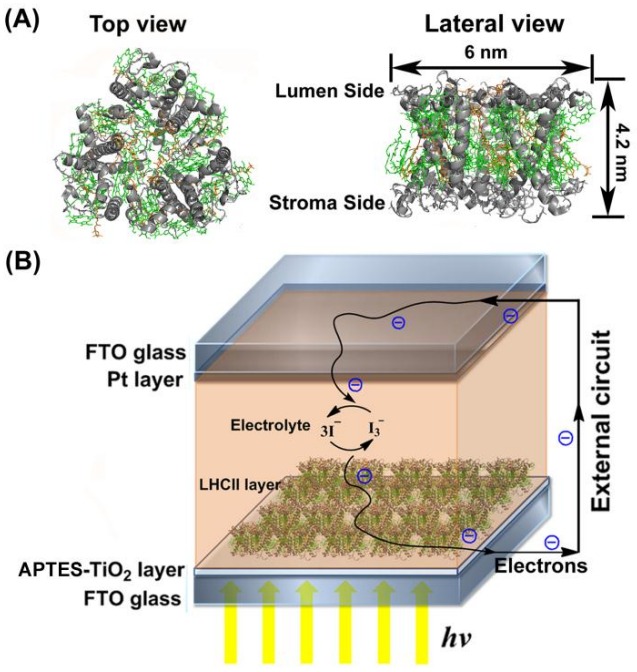

Figure 1. (A) Top and side view of the LHCII trimer consisting of Chl *a* and *b* (green); carotenoids (orange); and polypeptides (grey helices). (B) Schematic model of a LHCII sensitized solar cell assembled by attaching LHCII aggregates to a thin APTES-TiO_2 compact layer on a FTO-coated glass.

EXPERIMENTAL SECTION

Preparation of LHCII Aggregates. The LHCII trimers were extracted from spinach thylakoids as described in the literature[30] and were dispersed in 5 mM tricine buffer (pH = 7.5) with detergent (0.1 M sucrose and 0.06% n-dodecyl β-D-maltoside [β-DM]). Large aggregated LHCII complexes (called "large aggregates" throughout this paper) were formed upon removal of the detergent by several treatments with Biobeads SM-2 (Bio-Rad). For a comparison, smaller less quenched and more homogenous LHCII aggregates (called "small aggregates") were prepared by partial disaggregation of large aggregates in the buffer with low concentration of detergent (0.008% β-DM) after sonication.

The LHCII concentration shown in units of equivalent Chls, was measured according to the procedure described in reference.[31] Chls (Chl *a* and Chl *b*) in LHCII complexes were extracted with buffered aqueous acetone (80% aqueous acetone containing 2.5 mM phosphate buffer with pH = 7.8) and centrifuged with 7800 rpm to remove the insoluble protein residue. All the operations were handled quickly under dim light and 4 °C to avoid breakdown of the Chls. By measuring the UV-Vis absorption of the supernatant, the Chl content was calculated using the absorbance at 646.6 nm and 663.6 nm based on the equation shown in Table III of the reference[31] i.e. $\text{Chls}(a+b) = 17.6A^{646.6} + 7.34A^{663.6}$. Thus, the derived Chl contents of the small and large aggregate solutions were 16.2 μg Chl/mL and 17.1 μg Chl/mL, respectively.

Absorption and emission spectroscopic measurements. Absorption spectra were recorded using a Beckman DU640 at room temperature. Room-temperature fluorescence emission spectra of LHCII solutions were first measured with a 1-m McPherson monochromator (model 2601, slit width 100 μm) with 150/mm grating and a Princeton Instruments back-illuminated N_2-cooled CCD camera. The excitation source for the fluorescence experiments was a Coherent UV argon-

ion laser operating at 496.5 nm. Further fluorescence emission spectra was collected by a home-build set up from LHCIIs deposited on TiO_2/FTO photoanodes and LHCII solutions (for direct comparison). The excitation source was synchronously pumped dye laser (Spectra-Physics) equipped with cavity-dumper (Spectra-Physics) with the repetition rate of 4 MHz. The DCM (4-Dicyanomethylene-2-methyl-6-4-dimethylaminostyryl-4H-pyran) was used as a dye to provide the excitation wavelength at 663 nm. A micro-channel-plate photomultiplier (Hamamatsu) and a Jobin Yvon monochromator with 2 nm slit were used as the detection system.

Treatment of Photoanodes. Fluorine doped tin oxide (FTO) substrates (TEC8, Dyesol, Queanbeyan NSW, Australia) were covered with a thin TiO_2 layer (150-300 nm) by treatment with 40 mM aqueous solution of $TiCl_4$ at 75 °C for 20 minutes and sintered at 500 °C for 30 minutes, after rinsing with deionized water and ethanol. The obtained TiO_2-FTO and clean FTO substrates (for control experiments) were soaked in 10 wt% 3-aminopropyltriethoxysilane (APTES, 99% Sigma-Aldrich) in redistilled toluene, refluxed for 4 hours, followed by baking at 120 °C overnight. The APTES modified substrates were used as the photoanodes for LHCII-sensitized solar cells.

Fluorescence Microscopic Characterization of LHCII Attachment. APTES-FTO substrate masked with a TEM grid (1GC200, PELCO, Hole Width 90 μm; Bar Width 37 μm) was exposed to UV light (8 W UV lamp, 254 nm, Cole-Parmer) to create amino patterns. The amine groups under the exposed area were converted to –OH groups. After incubation in small-sized LHCII aggregate solution in dark at 4 °C for 12 hours followed by rinsing, fluorescence images were recorded with an Azioskop 2 FS Plus Microscope (Carl Zeiss) with a filter set of 480±20 nm excitation band and 515-565 nm emission band to examine the selective attachment of LHCII to amine-terminated surface.

Atomic force microscopy (AFM) Measurements. Clean Si wafers were soaked in the mixture of water, 30% ammonium hydroxide, 30% hydrogen peroxide (5:1:1 v/v ratio) at 75 °C for 15 min to make the wafers more hydrophilic, and then stored in an ultrapure water, dried by nitrogen blowing immediately before use. The pretreated Si wafer was dipped into LHCII solutions to immobilize some LHCII complexes and then rinsed with ultrapure water to remove the surfactant and other buffer residues. AFM was carried out in tapping mode on a BioScope (Digital Instruments, Santa Barbara, CA) with a scan speed at 1.5 Hz using silicon cantilevers with a resonance frequency between 65 and 80 kHz. The obtained images are processed with the software "Nanoscope III". For the line profiles, the software defines the mean height of the line as zero. The height of LHCII aggregate is represented by the difference between the peak and valley values in the line profiles.

Assembly of LHCII or Chlorophyll Sensitized Solar Cells. For LHCII-sensitized solar cells, an APTES-TiO_2-FTO or APTES-FTO substrate was used as a photoanode and the Pt-coated FTO/glass as the counter electrode. A 1 × 1 cm window was cut precisely into a 60 μm thick hot melt spacer (Solaronix, SX 1170-60PF) and was sealed at 110 °C for 5 min. The LHCII solutions were filled in the cell, which was stored in dark at 4 °C for 12 hours and then washed by successively injections of tricine buffer, water and ethanol. The electrolyte (Iodolyte AN-50, Solaronix) containing 50 mM iodide/tri-iodide in acetonitrile was finally injected into the cell to complete the solar cell fabrication. To avoid LHCII degradation, the Iodolyte electrolyte was replaced with related tricine buffer after each photovoltaic measurement, and the solar cells were stored at 4 °C. A similar solar cell using physisorbed Chls from spinach (≥ 90.0%, Sigma-Aldrich) (at 8:6 Chl *a* to Chl *b* molar ratio similar to LHCII) as alternative sensitizers was fabricated and used as a control. About 120 μg Chl/mL in dry diethyl ether was used as the

loading solution to sensitize TiO_2-covered FTO anode. The Iodolyte electrolyte was replaced with dry diethyl ether each time after photovoltaic measurements, and the Chl sensitized solar cell was stored at 4 °C before the next photovoltaic measurement.

Solar Cell Tests. Photovoltaic I-V curve of the solar cells was measured under the irradiation of 1 Sun power (100 mW/cm^2) using a 300 W Xeon lamp with an AM1.5G filter. Three different bandpass interference filters (Edmund Optics, 50 nm FWHM, OD >4.0, Stock NO. 84782, 86952, and 86954) were added to select light only in the wavelength range of 450±25 nm, 575±25 nm, and 675±25 nm, respectively, and photocurrent response curves were collected with chronoamperometry measurements using a potentiostat (CHI 440A Electrochemical Analyzer) while the shutter was turned on and off.

RESULTS AND DISCUSSION

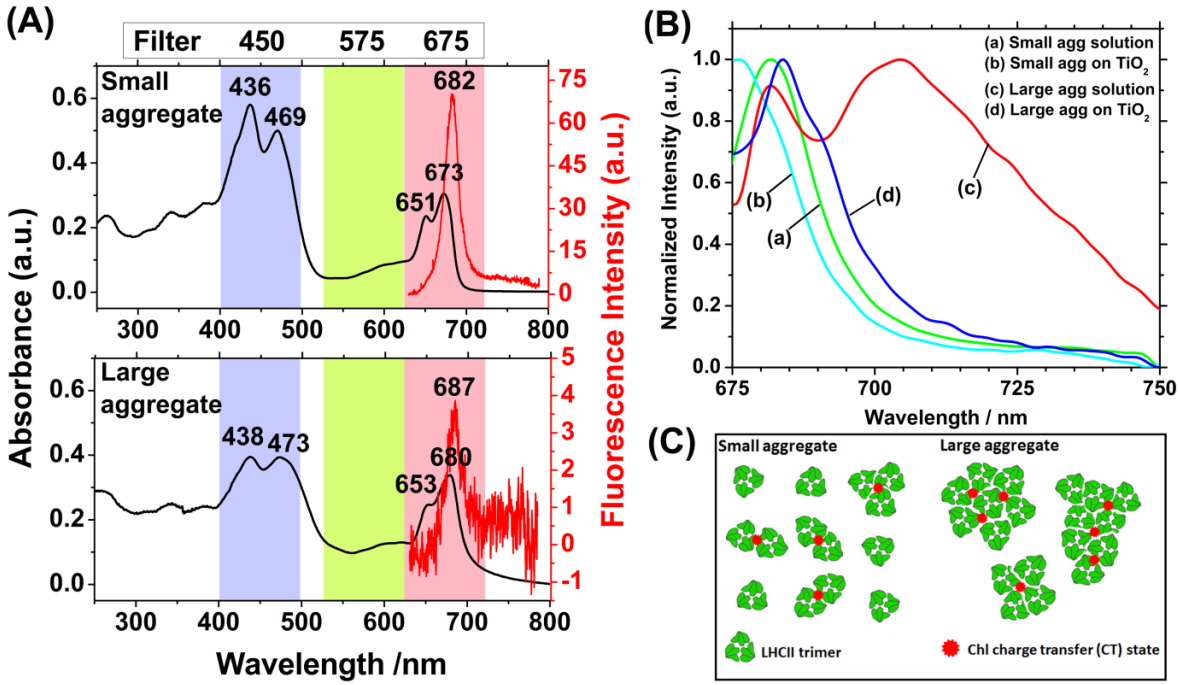

Figure 2. (A) Absorption and fluorescence emission spectra (λ_{ex} = 496.5 nm) of small- and large-size LHCII aggregates in tricine buffer with the concentration (in unit of total Chl content) of 16.2 µg Chl/mL and 17.1 µg Chl/mL, respectively. The colored shades indicate the bandwidth of the three bandpass interference filters used in photovoltaic measurements. (B) Normalized steady-state fluorescence emission spectra (λ_{ex} = 663 nm) of small- and large-size LHCII aggregates in solutions and deposited on the APTES-TiO_2-FTO photoanode surface. Note that the fluorescence of large aggregates on the TiO_2 surface is extremely weak. Each spectrum was normalized to its highest peak intensity for better view of the detailed spectroscopic features. (C) Schematic illustration of the CT states formed in small and large aggregates.

The absorption and fluorescence emission spectra of the small- and large-size LHCII aggregates are shown in the top and bottom frames of Figure 2A, respectively. Free Chl pigments in diethyl ether were reported to show strong absorption peaks in the Soret region (at 430 nm for Chl *a* and 452 nm for Chl *b*) and in the Q_y region (at 661 nm for Chl *a* and 645 nm for Chl *b*).[27] For the small-size LHCII aggregates in this study, these absorption peaks were red-shifted to 436/469 nm and 673/651 nm, respectively, similar to those observed in isolated LHCII trimers.[27] However, the room-temperature (0,0)-band emission was red-shifted by about 2-3 nm to 682-683 nm in contrast to isolated LHCII trimers with a maximum near 680 nm. The absorption of large-size aggregates shows larger red-shifts to 438/473 nm and 679/653 nm and a characteristic red tailing, suggesting the formation of CT states. The fluorescence of large LHCII aggregates is significantly quenched, displaying a tenth of the intensity in comparison to the small aggregates.

The raw spectra showed largely varied fluorescence intensity among LHCII samples with different degree of aggregation. For better view and comparison of their spectroscopic features, each spectrum was normalized to its highest peak intensity. Fig. 2B compares the normalized fluorescence emission spectra of LHCII in various aggregation states in solutions and after being deposited on the TiO_2/FTO photoanode as sensitizers. The fluorescence origin band shifts to about 687 nm in the large aggregates in solution (as compared to LHCII trimers which are not quenched) and a very strong far-red emission band (from 690 to 750 nm) appears. The far-red emission has been shown to derive from Chl-Chl CT states[11, 32], in agreement with the recent findings by Magdaong et al.[12] Formation of the CT states (characterized by a very strong electron-phonon (el-ph) coupling) was revealed recently via resonant HB spectroscopy.[29] In this case, resonant holes were burned in the low-energy absorption wing of aggregated LHCII complexes.[29] Thus the extent of the red-shift observed in room temperature fluorescence spectra and in particular the relative intensity of the far-red (from 690 to 750 nm) emission peak to the shorter-wavelength emission peak of aggregated LHCII complexes reflects the size of the aggregates and the quenching efficiency. This suggests that the large-size LHCII aggregates form CT states at much higher yield than the small-size aggregates.

Most interestingly, the CT state (far-red band) emission completely disappears when the aggregates are deposited as sensitizers on the surface of APTES-TiO_2-FTO substrates (to be used as photoanodes in solar cells) (Fig. 2B). Only very weak fluorescence remains. For small LHCII aggregates, the differences between the fluorescence emission spectra on APTES-TiO_2-FTO surface (curve b) and in solution (curve a) are much smaller. The shape of the fluorescence spectrum of small LHCII aggregates on TiO_2 is more similar to that of LHCII trimers in solution (but with largely different intensity, data not shown), while the fluorescence spectrum of large

aggregates on APTES-TiO_2-FTO surface is more red-shifted and differs pronouncedly (on top of the large difference in intensity).

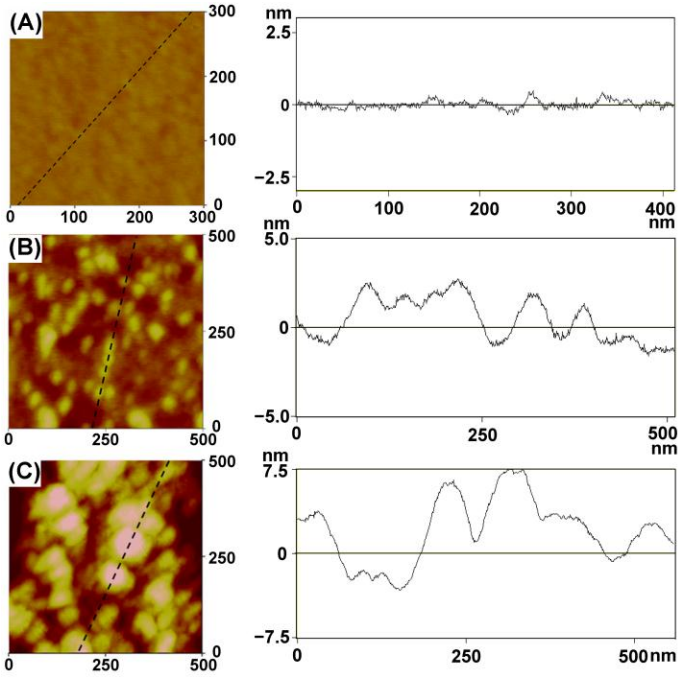

Figure 3. AFM images and line profiles of (A) a clean silicon wafer and a silicon wafer deposited with (B) the small-size LHCII aggregates and (C) the large-size LHCII aggregates. Measurements were carried out in tapping mode under a nitrogen atmosphere.

The size of aggregates in the above two samples was further confirmed by measuring the morphology of LHCIIs deposited on a flat surface with AFM, as shown in Figure 3. Compared to the smooth surface of bare silicon wafer (Figure 3A), brighter dots are clearly observed on the silicon wafer treated with the solution of small-size aggregates (Figure 3B). Two kinds of dots can be observed. The smaller (ca. 6 ~ 10 nm) and relative blurred ones are considered as intact LHCII trimers, while the larger (ca. 22 ~ 50 nm) and brighter ones would be small aggregates consisting of two or three trimers. Since the average height from the line profile in Figure 3B is only ~ 4 nm, LHCII in this sample likely only formed two dimensional aggregates. In contrast,

the AFM images of the large-size LHCII aggregates (formed by intentionally removing the detergent) revealed much larger islands with a diameter of 50 to 100 nm, as illustrated in Figure 3C. The line profile in Figure 3C shows a large height of ~10 nm, indicating the likely formation of three dimensional aggregates. These AFM images are consistent with the spectroscopic characteristics revealing the structural difference between the small- and large-size aggregates.

The physisorption of LHCII on the TiO_2 surface was found to be very weak and unstable, as indicated by the long incubation time (96 hours) required to reach saturated adsorption in literature.[27] We also found that only small amount of LHCII was anchored to the thin TiO_2 layer via physisorption, which significantly limited the photocurrent enhancement by LHCII sensitizers (see Figure S1 in the SI). It was recently reported that strong LHCII attachment can be obtained on a 3-aminopropyltriethoxysilane (APTES) functionalized FTO substrate via electrostatic interaction between the anionic residues on the stromal side with cationic $–NH_3^+$ groups.[26] This approach was adopted in this study. Figure 4A shows the fluorescence microscopic image of the small-size LHCII aggregates adsorbed on a patterned APTES-FTO substrate. The pattern correlates well with the shape of the optical mask (Figure 4B). The APTES-FTO surface was subjected to an UV exposure except in the cross-shaped area where the solid grid frame (ca. 37 μm in width) blocked the UV light. UV radiation is known to effectively cleave the amine group of APTES and to convert the surface back to normal –OH groups.[26] The fluorescence contrast between the exposed and blocked areas clearly confirmed that the electrostatic interaction facilitated by the APTES-functionalized surface provides much stronger LHCII adsorption. Hence, in this work, all the photoanode substrates for DSSCs were treated with APTES before LHCII attachment. The strong surface adsorption is particularly important in controlling sub-monolayer LHCII coverage on the APTES-TiO_2 surface. However, though

selective attachment of LHCII complexes was believed to occur between the anionic LHCII polypeptide at the stromal side and the cationic APTES surface,[26] it is likely that both stromal and luminal surfaces may work since they both contain negative charges in the LHCII proteins.

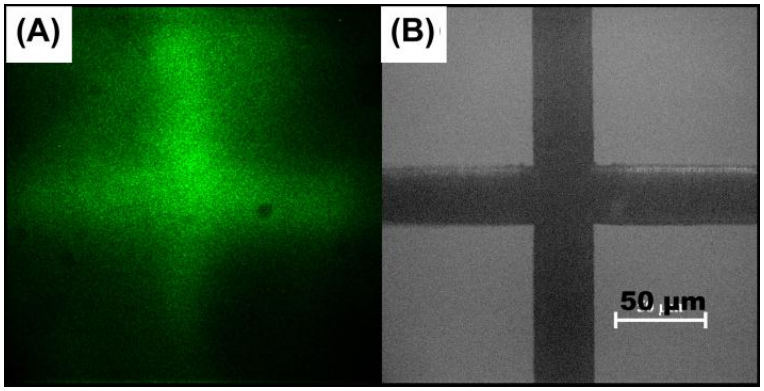

Figure 4. (A) A fluorescence image of small-size LHCII aggregates attached on a patterned APTES-FTO substrate. (B) An optical microscopy image of the corresponding mask in which the UV light was blocked by the solid grid frame (the dark area) and can only pass through the open squares (light areas). The scale bar is 50 μm.

In fabricating LHCII sensitized solar cells, a 1× 1 cm^2 window was cut in a 60 μm thick hot melt spacer sandwiched between the sensitized photoanode and a Pt/FTO/glass cathode. The total volume in the solar cell sealed with this spacer is ca. 6.0 μL. An isolated LHCII trimer has a cross-sectional area of 2618 to 3333 $Å^2$, corresponding to a radius of ~3 nm.[33] Assuming that all LHCIIs in solution are adsorbed onto the photoanode surface, it requires filling a LHCII solution with a concentration of 33.6 μg Chl/mL (in unit of equivalent Chl content) to form a hexagonal close-packed monolayer on 1 cm^2 TiO_2 surface, defined as $C_{monolayer}$. In order to study the effect of the aggregation-dependent CT states on the photovoltaic properties, more diluted samples were used to control the LHCII adsorption less than a fully covered monolayer. The actual concentration of LHCII solutions (C_{LHCII}) used in the experiments were calculated from

the optical absorbance of extracted chlorophylls (as described in the experimental section), giving 16.2 μg Chl/mL for small-size aggregates and 17.1 μg Chl/mL for large-size aggregates, both lower than that required concentration for forming a close-packed monolayer, i.e. *Cmonolayer* = 33.6 μg Chl/mL. Thus, it only forms a sub-monolayer if we fill the LHCII solution into the solar cell only one time. As schematically illustrated in Figure 2C, at such sub-monolayer stage, the adsorbed small- and large-size aggregates are isolated and not in contact with neighboring aggregates. The ET between the neighboring trimers/aggregates should be minimal.

To precisely determine the efficiency of LHCII adsorption onto the APTES-TiO_2 photoanode, we compared the extracted Chl concentration of the LHCII solution before and after incubation in solar cells (see Figure S2). The attachment efficiency (η_{attach}) was determined to be about 95%, which confirmed the strong electrostatic interaction between LHCII and APTES. As will be demonstrated later, such strong interaction also facilitates the high stability of the LHCII-sensitized solar cells. Thus the effective surface coverage (ESC, see Table 1) of LHCII on the photoanode of each solar cell can be estimated based on the following equation:

$$ESC = \frac{C_{LHCII}}{C_{monolayer}} \times \eta_{attach}\% \quad (1)$$

A full monolayer coverage (i.e., 100% of ESC) was attained by repeating 5 times the procedure including filling a fresh LHCII aggregate solution to the solar cell cavity, incubating for 4 hours for LHCII adsorption, and then rinsing off weakly bonded LHCII top layers with blank tricine buffer.

The emission spectra and AFM images discussed above clearly show that the two LHCII samples formed different extent of aggregates. We have shown recently that, in the case of large-

size aggregates (prepared in absence of detergent), more Chl-Chl CT states can be formed between the surface Chls as revealed by the very strong el-ph coupling.[29] The most relevant pigments involved in the formation of CT states are likely Chls 610, 611, and 612 (using nomenclature of Z. Liu et al.[5]) because they are close to the surface, have the lowest site-energies, and strongly contribute to the lowest energy exciton band.[34] Thus electrons transfer from the CT states to the TiO_2 layer facilitates generation of the observed photocurrent by aggregated LHCII.

If our interpretation is correct, we expect that the deposition of highly quenched large LHCII aggregates as a sensitizer and the functioning of this sensitizer as electron donor from the Chl-Chl CT states into the TiO_2 conduction band would concomitantly quench the far-red emission (from 690 to 750 nm) in the aggregates resulting from the Chl-Chl CT states. This is indeed the case as is seen in Fig. 2B. The far-red CT emission band is absent from the LHCII aggregates when deposited on TiO_2 and only a broad long-wave tail remains in the large aggregates.

Figure 1B schematically depicts the structure of the LHCII sensitized solar cell. One notable difference from the previous reported LHCII solar cells[26, 27] is that a very thin (150-300 nm) compact TiO_2 layer is used here to replace the 10 to 12 μm thick mesoporous TiO_2 film formed by sintering ~20 nm diameter TiO_2 nanoparticles. This is necessary for two reasons. First, it minimizes the photocurrent generated by UV photons absorbed by the TiO_2 framework. As shown in Figure S3A, a solar cell fabricated with a bare 10-μm mesoporous TiO_2 can generate by itself a strong photovoltaic effect with a short-circuit photocurrent (J_{SC}) from ~0.14 to ~0.6 mA/cm^2 under 1 sun illumination. This makes it difficult to extract the photocurrent generated explicitly by LHCII sensitizers. Second, the internal pores of the typical mesoporous TiO_2 films are tortuous and poorly defined, with the size of only ~8 nm or less. As a result, it was reported

that even the isolated LHCII trimers, which have a comparable size to the pore, only formed a layer at the outer surface of the mesoporous TiO_2 film.[27] Both of these factors may obscure the details of LHCII contribution, particularly at the sub-monolayer coverage and in the I-V curve under the irradiation of the full solar spectrum.

On the other hand, a thin compact TiO_2 layer is required as a barrier to prevent electron backflow from the FTO anode to the electrolyte. Figure S3B shows that the DSSC with LHCII directly attached to the APTES-FTO anode only gives very low values for both J_{SC} and open-circuit voltage (V_{OC}). In a previous report[35], we have demonstrated that a TiO_2 film of 150 to 300 nm thickness formed by treatment of the FTO electrode with 40 mM $TiCl_4$ solution for 20 minutes serves well as an effective barrier layer. This method was adopted in this study. In addition, to avoid protein denaturation by the volatile organic solvent (such as acetonitrile) that was used in typical Grätzel cells, we previously used an ionic liquid electrolyte. However, we found that, though clear photovoltaic effects were observed, the performance of the ionic liquid electrolyte is far inferior to the volatile electrolyte (see Figure S4 in the SI). Hence the typical Iodolyte in acetonitrile, which was recently reported to be compatible with LHCII complexes[27], was used in this study.

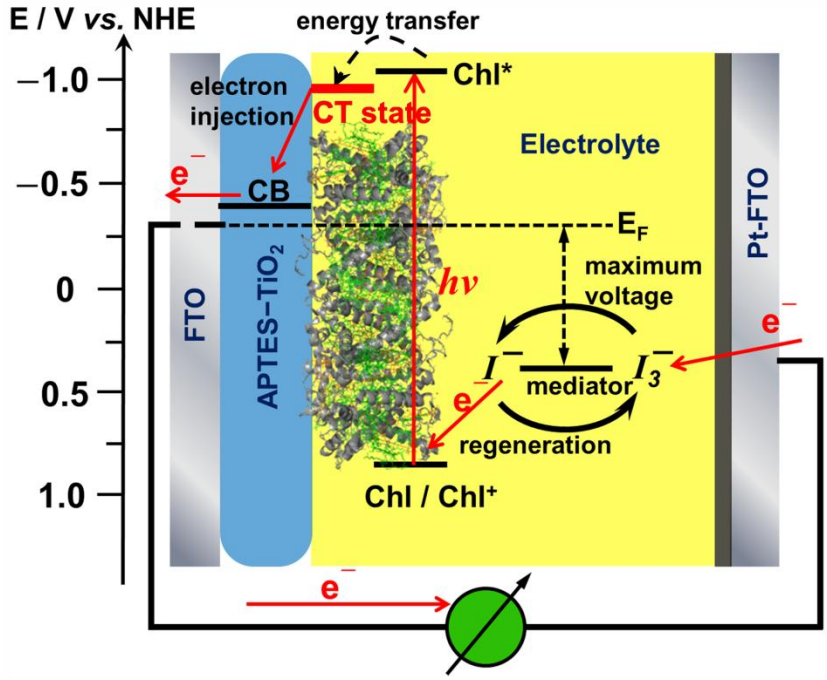

Figure 5. Electron transfer and energy level scheme of a photovoltaic device based on aggregated LHCII complexes.

Figure 5 shows the electron transfer and energy level scheme of the prepared solar cell based on aggregated LHCII complexes as the sensitizer. Potentials are relative to the normal hydrogen electrode (NHE). The V_{OC} (maximum voltage) corresponds to the difference between the redox potential of the Iodolyte mediator and the Fermi level of the FTO film. To be noted, the CT states in aggregated LHCII mixed with the excited state of chlorophylls have lower oxidation potential due to their more reddish absorption and red tail in UV spectra (see Fig. 2 and the related description). The CT states couple with the TiO_2 conduction band more effectively and lead to a more efficient electron injection accompanied with fluorescence emission quench (as shown in Fig. 2B).

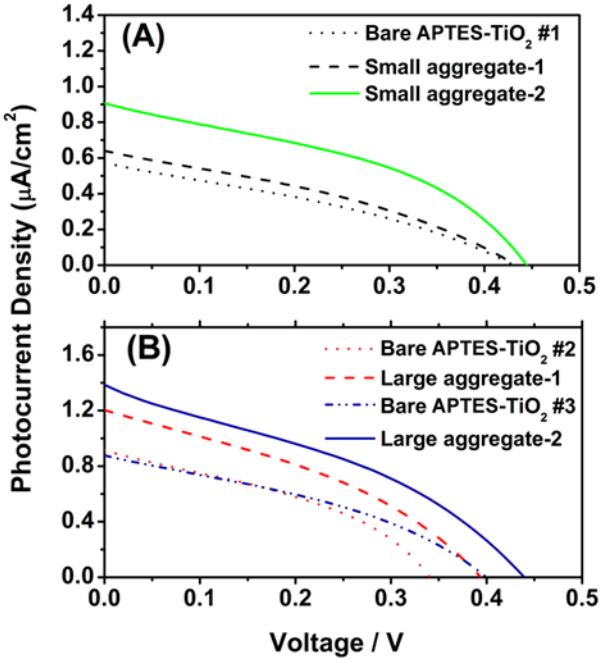

Figure 6. I-V curves of LHCII sensitized TiO_2 solar cells. (A) Solar cells made of a bare APTES-TiO_2 photoanode (bare APTES-TiO_2 #1, dot) and after being first sensitized with 45.8%-coverage small-size LHCII aggregates (small aggregate-1, dashed line) and then further sensitized with 100%-coverage small-size LHCII aggregates (small aggregate-2, solid). (B) Solar cells made of the 2nd bare APTES-TiO_2 photoanode (bare APTES-TiO_2 #2, dot) and this electrode after being sensitized with 48.3%-coverage large-size LHCII aggregates (large-size aggregate-1, dash), the 3rd bare APTES-TiO_2 photoanode (bare APTES-TiO_2 #3, dash-dot-dot) and this electrode after being sensitized with high-coverage large-size LHCII aggregates (large-size aggregate-2, solid). All measurements were carried out under 1 sun illumination with an AM1.5G filter.

Figure 6 shows I-V curves of the TiO_2 solar cells sensitized with the two LHCII samples with different degrees of aggregation and at two different ESCs, one submonolayer and one full monolayer. These data confirmed that the photovoltaic effects were enhanced after the APTES-TiO_2 surface was sensitized with both small- and large-size LHCII aggregates. Both J_{SC} and V_{OC}

consistently increased as the ESC of LHCII aggregates was raised. Modifying the surface of the TiO_2 thin film with APTES suppressed the photocurrent generated by UV photon absorption in TiO_2, with J_{SC} dropping from ~8 μA/cm^2 (see Figure S1) to ~0.6 to 0.9 μA/cm^2, possibly due to electron trapping and recombination at the positively charged $–NH_3^+$ group at the TiO_2 surface. However, as it is shown later, the $–NH_3^+$ group did not block the CT from LHCII to the photoanode since illumination the solar cell with the selected light band that can only be absorbed by LHCII was able to produce substantial photocurrent. APTES modification was necessary to enable the strong adsorption of LHCII on the TiO_2 surface and thus made it possible to observe the differences between two LHCII aggregates. The values of V_{OC} are comparable in all these solar cells, at about 0.40 to 0.45 V.

Table 1. The characteristic values of the TiO_2 solar cells sensitized with LHCII aggregates at different ESCs (in percentage).

	ESC%*	J_{SC} (μA/cm^2)	V_{OC} (V)	ΔJ_{SC}%
Bare APTES-TiO_2 #1	0	0.575	0.427	N.A.
Small aggregate-1	45.8	0.640	0.432	11.3
Small aggregate-2	100	0.907	0.444	57.7
Bare APTES-TiO_2 #2	0	0.915	0.340	N.A.
Large Aggregate-1	48.3	1.203	0.394	31.5
Bare APTES-TiO_2 #3	0	0.876	0.398	N.A.
Large Aggregate-2	100	1.386	0.424	58.2

Table 1 summarizes the characteristic values of the I-V measurements shown in Figure 6. The percentage increase in J_{SC} (i.e., ΔJ_{SC}%) from the bare APTES-TiO_2 cell was used to compare the results so that the difference caused by the variation in thickness and roughness of the TiO_2

barrier layer can be normalized. By filling LHCII solution into the cell only once, the LHCII adsorption was defined by Eq. (1), giving an ESC of 45.8% for small-size aggregates (in the cell labeled as "small aggregate-1") and 48.3% for large-size aggregates (in the cell labeled as "large aggregate-1"). Though the ESCs are similar, the ΔJ_{SC}% value with the large-size aggregate is almost 3 times that of the small-size aggregate (31.5% vs. 11.3%). The larger enhancement is likely related to the higher extent of CT states formed in large-size aggregates and the resulted more efficient electron injection from CT states to the TiO_2.

Interestingly, at the full monolayer coverage (i.e., 100% ESC), the solar cells sensitized with both small- and large-size LHCII aggregates (i.e., "small aggregate-2" and "large aggregate-2") showed almost the same ΔJ_{SC}% values (57.7% vs. 58.2%). Since the packing density of the LHCII trimer on the TiO_2 surface is nearly the same, no matter if they are originally from small- or large-size aggregates, the CT states at this condition are about the same as well. It is noteworthy that the power conversion efficiency is increased by ~58% from the bare APTES-TiO_2 cell after being sensitized with a full monolayer of LHCII aggregates, which is higher than the 35% increase using LHCII trimers as a sensitizer on the 10 μm thick mesoporous TiO_2 film[27].

To identify the origin of the photocurrent generation, the synchronous response of J_{SC} to the illumination of the full solar spectrum and in selected wavelength bands were recorded and illustrated in Figure 7. The current density is normalized to the photocurrent of the solar cell with bare APTES-TiO_2 photoanodes in order to correct the variation of TiO_2 photoanode (see Figure S5 in the SI for normalization processing). All photocurrents were highly reproducible as the illumination was turned on and off for four cycles. Only a very slow drift was observed during the illumination *on,* indicating that LHCII complexes were stable under the experimental conditions and were effectively regenerated by iodide/tri-iodide redox electrolyte. Under 1 sun

illumination with the full solar spectrum (Figure 7A), all curves showed higher photocurrent after LHCII sensitization, fully consistent with the I-V measurements in Figure 6. The cell "large aggregate-1" (ESC = 48.3%) gave significantly higher normalized current density than "small aggregate-1" (ESC = 45.8%), though both of them had similar level of LHCII coverage. The curves for the cells with the full LHCII monolayer coverage, i.e., "small aggregate-2" and "large aggregate-2", are essentially overlapped with each other.

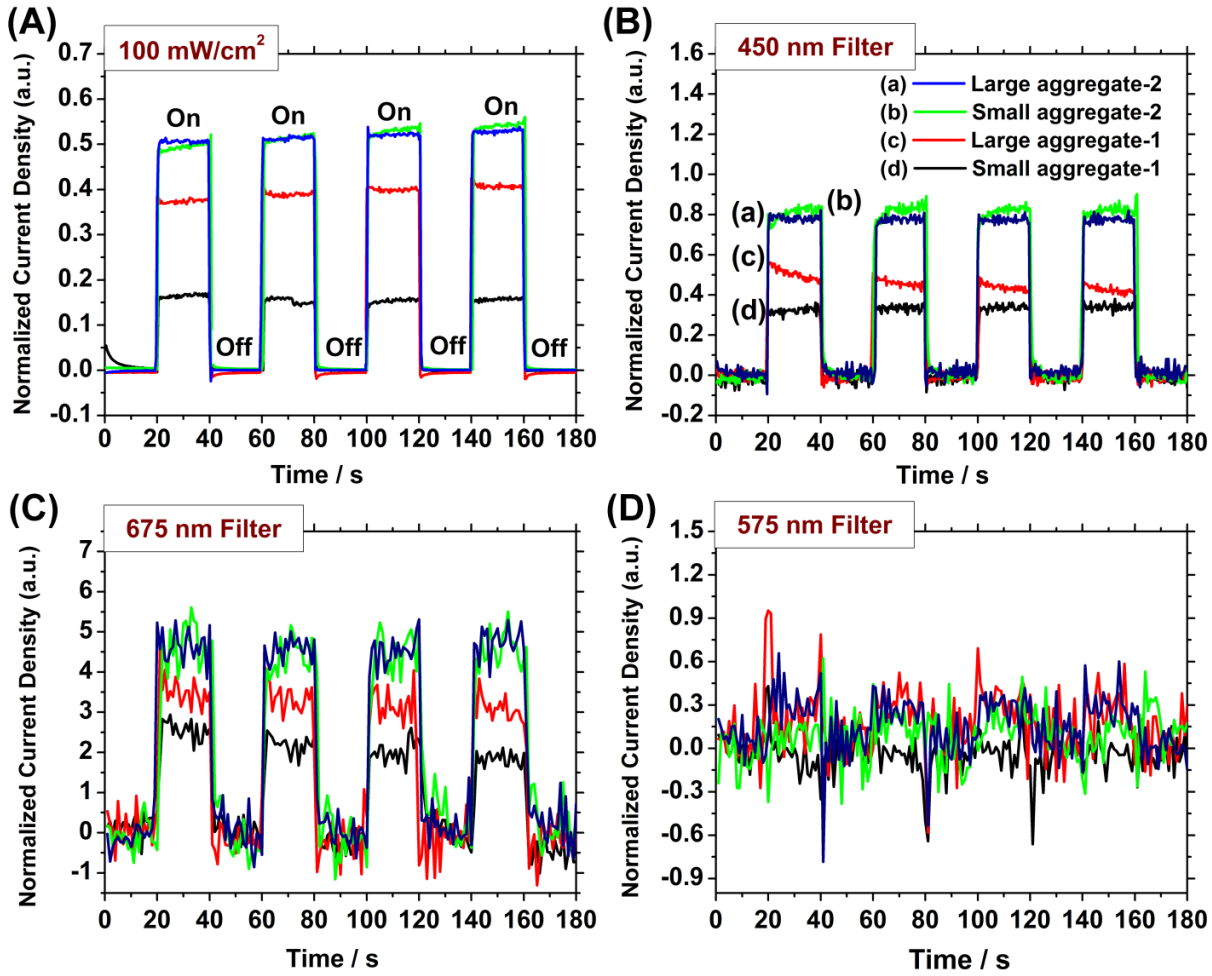

Figure 7. Synchronous photocurrent response of the TiO_2 solar cells sensitized with different ESC% of small- and large-sized LHCII aggregates under 1 sun illumination with the full solar spectrum (A) and passing through bandpass interference filters at 450±25 nm (B); 675±25 nm

(C); and 575±25 nm (D). The photocurrents were normalized as described in the SI (see Figure S5). "On" and "Off" refer to illuminated and dark conditions, respectively.

In addition to the full solar spectrum, three bandpass interference filters were applied to limit the illumination to three narrow wavelength regions. The chosen illumination ranges are 450±25 nm (Soret region of Chls), 675±25 nm (Q_y region of Chls), and 575±25 nm (region with minimum absorbance), in accordance with the shaded areas in the LHCII absorption spectra shown in Figure 2. Figures 7B and 7C clearly demonstrated that the photocurrent response can be attributed to the absorbance of LHCII proteins. The correlation of the photocurrent magnitude and the LHCII coverage, as well as the degree of aggregation, agreed well with that of the full solar spectrum. The illumination in the 575±25 nm region, which has minimum photon absorption by LHCII, however, did not generate any photocurrent (Figure 7D).

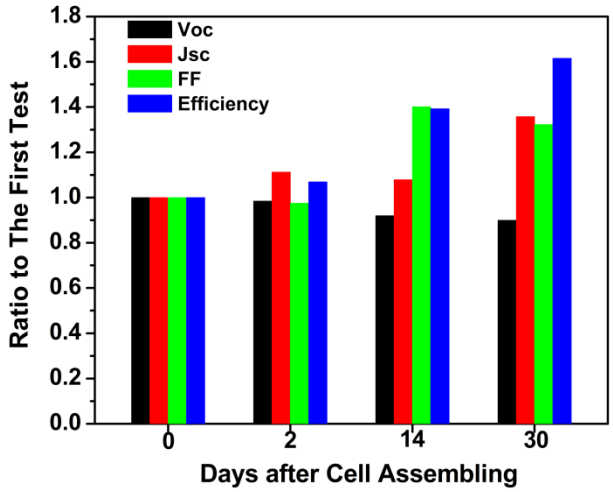

Figure 8. The performance characteristics of LHCII-sensitized TiO_2 solar cells measured over 30 days after assembly. All parameters were normalized to the value obtained with the cell immediately after it was assembled.

Proteins are normally unstable and tend to denature in organic solvents such as acetonitrile. However, we found that LHCIIs were extremely robust (regarding photocurrent generation) after they were attached to the APTES-TiO_2 surface, which was critical for LHCII-sensitized solar cell to work well in acetonitrile based Iodolyte. That is, a possible denatureration (that cannot be fully excluded) did not affect the performance of our photovoltaic devices. Figure 8 illustrates the characteristic photovoltaic properties of the solar cell "Small aggregate-1" (i.e., 45.8% ESC of small-size LHCII aggregates) over 30 days after assembly. In fact, not only did the cell display an outstanding stability, but the overall cell performance improved with time as demonstrated by the increase in J_{SC}, fill-factor (*FF*), and power conversion efficiency (η). Only V_{OC} slightly decreased. In these experiments, the only effort to avoid cell degradation was to replace Iodolyte with tricine buffer after each photovoltaic measurement and store them at 4º C before refilling Iodolyte for the next measurement. Continued reorganization of LHCII complexes could occur during this period, allowing more CT states formation or a better contact to the TiO_2 surface, leading to an improved cell performance.

To further understand the effects of LHCII reorganization, a TiO_2 solar cell sensitized with isolated chlorophyll pigments was also prepared and tested by the same procedure as a control. Since Chl *a* and Chl *b* are the two major light-harvesting pigments in LHCII complex (with a molar ratio of 8 : 6), the bare TiO_2 solar cell was thus sensitized in a dry diethyl ether solution with a total Chl concentration of 120 μg Chl/mL at 8:6 molar ratio of.Chl *a* and Chl *b*. As shown in Figure S6 of the SI, although Chls did enhance the photocurrent of the solar cell at the beginning, the current kept decreasing in the following 5 days (120 hours). The current response curves illustrated that the contribution of Chls to photocurrent almost became negligible after 72 hrs. It should be noted that Chls attached onto the TiO_2 layer only through weak physisorption

tend to desorb over time and are easily oxidized in atmosphere. Compared with the LHCII-sensitized solar cells discussed above, the stability of the Chl-sensitized solar cell was very poor, which illustrated the necessity of using photosynthetic protein complexes instead of Chl pigments alone.

CONCLUSIONS

LHCII complexes with different degrees of aggregation were respectively applied onto a model thin film TiO_2 solar cell. The results not only illustrated that LHCII can serve as a remarkably stable photosensitizer for DSSCs, but also revealed that the photovoltaic properties of this system, represented by the photocurrent enhancement, can be directly correlated to the aggregation induced charge transfer (CT) states. The existence of the CT states must have improved the electron injection into TiO_2, since the photocurrent generated by large-size LHCII aggregates was significantly higher than the same amount of small-size LHCII aggregates. We emphasize that formation of CT states in aggregated LHCII complexes is consistent with the observed strong electon-phonon coupling and much weaker (red-shifted) fluorescence emission observed in aggregated LHCII complexes at low temperatures.[29] More CT states formed by a possible LHCII reorganization or a better contact to the photoanode are likely responsible for the high stability and continuously increased performance of the solar cell after assembling. Our LHCII sensitized solar cell adopted a thin film design to reduce the background current from the traditional mesoporous TiO_2 layer and amplify the contribution from sensitizing protein complexes. This design should be also applicable to other photosynthetic protein complexes, which provides a new platform to tap into the early biophysical processes of photosystems, i.e., the photon capture and energy/charge transfer.

ASSOCIATED CONTENT

Supporting information includes (1) photovoltaic I-V curves of physisorbed LHCII large aggregates on bare thin-film TiO_2/FTO anodes, (2) UV-vis absorption spectra of acetone extracted Chls from the solution before and after filling into the solar cells, (3) photovoltaic I-V curves of control solar cells with various photoanodes including a bare 10 μm thick TiO_2 nanoparticle film, APTES modified FTO photoanodes with and without LHCII sensitization), (4) photovoltaic I-V curves and synchronous photocurrent response during light on/off with LHCII-sensitized solar cells in ionic liquid electrolyte, (5) synchronous photocurrent response curves of an APTES-TiO_2 solar cell before and after being sensitized with small-size LHCII aggregates, and (6) stability tests of solar cells sensitized with physisorbed isolated Chls.

AUTHOR INFORMATION

Corresponding Author

*Emails: (Jun Li) junli@ksu.edu, (Ryszard Jankowiak) ryszard@ksu.edu

Notes

The authors declare no competing financial interest.

ACKNOWLEDGMENT

This work was supported by the NSF EPSCoR Award EPS-0903806 (including the matching support from the State of Kansas through Kansas Technology Enterprise Corporation) to J.L. and R.J. We thank Adam Kell (KSU) and Yichen Zheng (KSU) for insightful discussion and comments. A.R.H. acknowledges the EU Training and Research Network "Harvest" and the Deutsche Forschungsgemeinschaft (DFG HO-924/3-1) for grants.

REFERENCES

1. D. Gust, T. A. Moore and A. L. Moore, *Acc. Chem. Res.*, 1993, 26, 198-205.

2. M. Sykora, K. A. Maxwell, J. M. DeSimone and T. J. Meyer, *PNAS*, 2000, 97, 7687-7691.

3. J. H. Alstrum-Acevedo, M. K. Brennaman and T. J. Meyer, *Inorganic Chemistry*, 2005, 44, 6802-6827.

4. S. Caffarri, R. Kouřil, S. Kereïche, E. J. Boekema and R. Croce, *EMBO J.*, 2009, 28, 3052-3063.

5. Z. Liu, H. Yan, K. Wang, T. Kuang, J. Zhang, L. Gui, X. An and W. Chang, *Nature*, 2004, 428, 287-292.

6. M. P. Johnson, T. K. Goral, C. D. P. Duffy, A. P. R. Brain, C. W. Mullineaux and A. V. Ruban, *Plant cell.*, 2011, 23, 1468-1479.

7. A. R. Holzwarth, Y. Miloslavina, M. Nilkens and P. Jahns, *Chem. Phys. Lett.*, 2009, 483, 262-267.

8. E. Belgio, C. D. P. Duffy and A. V. Ruban, *Physical Chemistry Chemical Physics*, 2013, 15, 12253-12261.

9. A. V. Ruban, R. Berera, C. Ilioaia, I. H. M. van Stokkum, J. T. M. Kennis, A. A. Pascal, H. van Amerongen, B. Robert, P. Horton and R. van Grondelle, *Nature*, 2007, 450, 575-578.

10. A. R. Holzwarth and P. Jahns, *NPQ mechanisms in intact organisms as derived from ultrafast fluorescence kinetics studies*, Springer Science, Advances in Photosynthesis and Respiration, 2014.

11. Y. Miloslavina, A. Wehner, P. H. Lambrev, E. Wientjes, M. Reus, G. Garab, R. Croce and A. R. Holzwarth, *FEBS Letters*, 2008, 582, 3625-3631.

12. N. Magdaong, M. Enriquez, A. LaFountain, L. Rafka and H. Frank, *Photosynth Res*, 2013, 118, 259-276.

13. B. O' Regan and M. Grätzel, *Nature*, 1991, 353, 737-740.

14. V.-D. Dao, S.-H. Kim, H.-S. Choi, J.-H. Kim, H.-O. Park and J.-K. Lee, *J. Phys. Chem. C*, 2011, 115, 25529-25534.

15. M. Law, L. E. Greene, J. C. Johnson, R. Saykally and P. Yang, *Nat Mater*, 2005, 4, 455-459.

16. J. Qi, X. Dang, P. T. Hammond and A. M. Belcher, *Acs Nano*, 2011, 5, 7108-7116.

17. G. K. Mor, K. Shankar, M. Paulose, O. K. Varghese and C. A. Grimes, *Nano Lett.*, 2005, 6, 215-218.

18. S. Saha, S. Sarkar, S. Pal and P. Sarkar, *J. Phys. Chem. C*, 2013, 117, 15890-15900.

19. A. Yella, H.-W. Lee, H. N. Tsao, C. Yi, A. K. Chandiran, M. K. Nazeeruddin, E. W.-G. Diau, C.-Y. Yeh, S. M. Zakeeruddin and M. Grätzel, *Science*, 2011, 334, 629-634.

20. J. Burschka, N. Pellet, S.-J. Moon, R. Humphry-Baker, P. Gao, M. K. Nazeeruddin and M. Grätzel, *Nature*, 2013, 499, 316-319.

21. R. Das, P. J. Kiley, M. Segal, J. Norville, A. A. Yu, L. Wang, S. A. Trammell, L. E. Reddick, R. Kumar, F. Stellacci, N. Lebedev, J. Schnur, B. D. Bruce, S. Zhang and M. Baldo, *Nano Lett.*, 2004, 4, 1079-1083.

22. M.-J. den Hollander, J. G. Magis, P. Fuchsenberger, T. J. Aartsma, M. R. Jones and R. N. Frese, *Langmuir*, 2011, 27, 10282-10294.

23. A. Sumino, T. Dewa, N. Sasaki, M. Kondo and M. Nango, *J. Phys. Chem. Lett.*, 2013, 4, 1087-1092.

24. D. Gerster, J. Reichert, H. Bi, J. V. Barth, S. M. Kaniber, A. W. Holleitner, I. Visoly-Fisher, S. Sergani and I. Carmeli, *Nat Nano*, 2012, 7, 673-676.

25. M. R. Narayan, *Renew. Sust. Energ. Rev.*, 2012, 16, 208-215.

26. M. Nagata, M. Amano, T. Joke, K. Fujii, A. Okuda, M. Kondo, S. Ishigure, T. Dewa, K. Iida, F. Secundo, Y. Amao, H. Hashimoto and M. Nango, *ACS Macro Letters*, 2012, 1, 296-299.

27. D. Yu, G. Zhu, S. Liu, B. Ge and F. Huang, *International Journal of Hydrogen Energy*, 2013, 38, 16740-16748.

28. A. Mershin, K. Matsumoto, L. Kaiser, D. Yu, M. Vaughn, M. K. Nazeeruddin, B. D. Bruce, M. Graetzel and S. Zhang, *Sci. Rep.*, 2012, 2.

29. A. Kell, X. Feng, C. Lin, Y. Yang, J. Li, M. Reus, A. R. Holzwarth and R. Jankowiak, *J. Phys. Chem. B*, 2014, 118, 6086-6091.

30. P. H. Lambrev, Z. Várkonyi, S. Krumova, L. Kovács, Y. Miloslavina, A. R. Holzwarth and G. Garab, *Biochimica et Biophysica Acta (BBA) - Bioenergetics*, 2007, 1767, 847-853.

31. R. J. Porra, W. A. Thompson and P. E. Kriedemann, *Biochimica et Biophysica Acta (BBA) - Bioenergetics,* 1989, 975, 384-394.

32. M. G. Müller, P. Lambrev, M. Reus, E. Wientjes, R. Croce and A. R. Holzwarth, *ChemPhysChem*, 2010, 11, 1289-1296.

33. W. a. I. Gruszecki, E. Janik, R. Luchowski, P. Kernen, W. Grudzinski, I. Gryczynski and Z. Gryczynski, *Langmuir*, 2009, 25, 9384-9391.

34. T. Renger, M. E. Madjet, A. Knorr and F. Müh, *J. Plant Physiol.*, 2011, 168, 1497-1509.

35. Y. Zheng, S. Klankowski, Y. Yang and J. Li, *ACS Appl. Mater. Interfaces*, 2014, In press.